Modeling of Electronic Mobilities in Halide Perovskites: Adiabatic Quantum Localization Scenario

Antoine Lacroix,[1,*] Guy Trambly de Laissardière,[2,†] Pascal Quémerais,[1,‡] Jean-Pierre Julien,[1,§] and Didier Mayou[1,‖]
[1]Université Grenoble Alpes, CNRS, Institut NEEL, F-38042 Grenoble, France
[2]CY Cergy Paris Université, CNRS, Laboratoire de Physique théorique et Modélisation, F-95302 Cergy-Pontoise, France

(Received 20 December 2019; accepted 9 April 2020; published 12 May 2020)

The transport properties of MAPbI3 are analyzed within a tight-binding model. We find a strong Fröhlich interaction of electron and holes with the electrostatic potential induced by the longitudinal optical phonon modes. This potential induces a strong scattering and limits the electronic mobilities at room temperature to about 200 $cm^2/V\,s$. With additional extrinsic disorder, a large fraction of the electrons and holes are localized, but they can diffuse by following nearly adiabatically the evolution of the electrostatic potential. This process of diffusion, at a rate which is given by the lattice dynamics, contributes to the unique electronic properties of this material.

DOI: 10.1103/PhysRevLett.124.196601

Metal halide perovskites have recently emerged as great materials for photovoltaic and optoelectronic devices [1,2]. The rapid progresses obtained in these applications require also to gain a better fundamental understanding of their electronic properties. In particular, there is so far no consensus on the mechanism of charge transport in these materials [3,4]. For good crystals below the Debye temperature, one expects the formation of a large polaron due to the coupling to longitudinal optical (LO) modes. Although the mass renormalization, estimated to about 40%, is moderate, this polaronic effect is often considered in the literature [5–7]. However, owing to the very low phonons frequency and to anharmonicity, a strong dynamic disorder develops above the Debye temperature (175 K in MAPbI3) [8–11] and it is not clear whether the large polaron state survives at room temperature. Theoretical investigations point toward the importance of the scattering of charge carriers by LO phonon modes [12,13]. The dipolar moment of the methylammonium (MA) has also been considered as a possible source of scattering, even though recent calculations suggest that the scattering by the associated dipolar field has a limited effect on transport [14]. Other sources of scattering have also been considered related to the anharmonic behavior of these crystals at room temperature [15]. Extrinsic disorder is of course present in real systems, but its effect is difficult to model.

In this Letter, we investigate the transport properties of electrons and holes in $MAPbI_3$ (MAPI) within a tight-binding model, which allows us to perform calculations of quantum diffusion in real space [16–19]. We take into account the effect of intrinsic thermal disorder of the PbI_3 matrix, as well as the dipolar electric field created by the MA cation. The Drude-Anderson model [20] allows us to rationalize the numerical results and to extract the fundamental parameters of electronic transport. At room temperature, the results show that the broadening of the electronic states due to the sources of disorder is much larger than the formation energy of the polaronic state. Therefore, the polaronic effect should play a minor role at room temperature, and the mobilities are determined mainly by the Fröhlich scattering and by quantum localization effects. This quantum localization has experimental signatures that can be close to those of a polaronic state, for example, with terahertz optical conductivity. The dynamic thermal disorder tends to break the quantum localization by dephasing, which allows charge carrier diffusion. This process of diffusion is neither a bandlike process, nor a thermally activated hopping and contributes to the unique properties of this material.

We use a tight-binding model with parameters fitted [21] to be consistent with MAPI's *ab initio* band structure calculations [22,23]. The thermal disorder induces off-diagonal and diagonal disorders.

The off-diagonal disorder is related to the variation of the distance and overlapping between orbitals. We describe atomic displacements using independent Einstein oscillators, where all atomic displacements are statistically independent, with harmonic and isotropic potentials. Such single particle potentials have been computed from experimental data by Tyson *et al.* [24]. We generate an atomic configuration and recompute the orbital couplings from the Slater-Koster relations [25] for changes in direction and via a power law in $(d_0/d)^2$ for changes in distance.

The diagonal disorder of the on-site energies is determined by the electrical potential inside the material. The variation of this electrical potential with respect to the periodic structure is caused by the displacement of the charged ions and the orientation of the MA molecules. However, the contribution of the MA molecules is found to be small [14], as shown in the Supplemental Material [26–31], and with negligible

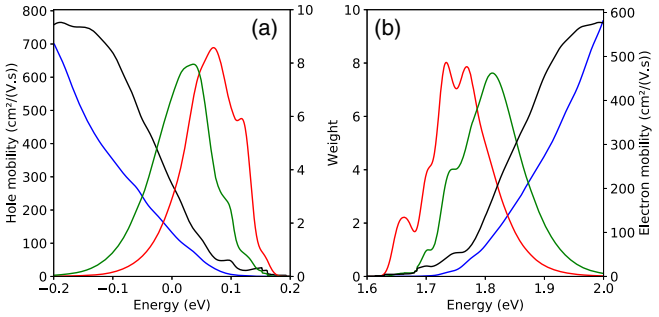

FIG. 1. Variations of carrier mobilities (black), density of states (blue), occupied DOS (red), and differential conductivity (green) as a function of energy, near band edges, for (a) holes and (b) electrons. Except for mobility, the quantities are normalized such that their integral is one on the energy interval (weight axis).

effects on mobilities. Therefore, we present results only with diagonal disorder due to the displacement of the lead and iodine ions. The displacement of an atom creates a dipole moment equal to the product of the displacement by the Born charge in the considered direction. We use the Born charges computed by Pérez-Osorio *et al.* [10]. The main contribution to the electrostatic potential is expected to come from the LO phonon modes, for which the energies are in the 10–13 meV range [12]. Here we also represent the statistics of the displacements by using an Einstein model with an effective phonon pulsation $\omega_E \simeq 10$ meV.

From the relation between the dipolar moments $\vec{d}_i$, k_bT, and ω_E, we find (see Supplemental Material [26]) that the variable $W = k_bT/(\varepsilon_r\omega_E)^2$ is the only parameter determining the statistics of the electrostatic potential. In the rest of the Letter, unless otherwise specified, we fix the temperature to $T = 300$ K and the relative dielectric constant to $\varepsilon_r = 5$ [32]. The value of ω_E that best reproduces the gap at room temperature is close to 10 meV (see Supplemental Material [26]) and we discuss only the effect of varying ω_E around 10 meV. Disorder thus increases when ω_E decreases. The central idea of this study is that the transport properties are mainly determined by a single parameter (ω_E or W), representing the strength of disorder and the scattering rate.

We first present results for $\omega_E = 10$ meV showing energy resolved analysis for the properties of electrons and holes. Figure 1 shows the density of states (DOS) $n(E)$, the occupied density of states $n(E)\exp(-\beta E)$, the mobility $\mu(E)$ at energy E, and the differential conductivity $d\sigma/dE = \mu(E)n(E)\exp(-\beta E)$. We find that the occupied DOS is important within a range of about 0.2 eV and that states contributing the most to the transport of current are also within a range of about 0.2 eV, but slightly shifted away from the band edges. The very small mobility close to the band edge is related to Urbach's tail, which cannot be analyzed with the present energy resolution of 10–20 meV (see Supplemental Material [26]). The typical values of mobility for the states that contribute most are in the 100–300 $\mathrm{cm}^2/\mathrm{V\,s}$ range, which corresponds indeed to the best experimental mobilities. Finally, we note that the density of states of both electrons and holes are very different from the parabolic shape typical of free particles with an effective mass. This indicates that the disorder is strong and that the energy broadening of a state due to the disorder is comparable to its energy, counted from the band edge. According to the Ioffe-Regel criterion [33], one expects important quantum localization effects that we consider now.

We start our analysis of the quantum localization effects by considering an extension of the Drude-Anderson model [20]. Two fundamental quantities for the quantum transport are the mean squared displacement $X^2(t)$ and the velocity correlation function $C(t)$ that are defined for each type of carrier (electrons and holes). They are related by

$$\frac{1}{2}\frac{dX^2(t)}{dt} = \int_0^t C(t')dt'. \tag{1}$$

Using the Kubo formalism, one can derive the optical terahertz conductivity $\sigma(\omega)$ from $C(t)$ or $X^2(t)$ [20,34,35],

$$\sigma(\omega) = e^2 n \frac{\tanh(\beta\hbar\omega/2)}{\hbar\omega/2}\,\mathrm{Re}\int_0^\infty e^{i\omega t}C(t)dt, \tag{2}$$

where e and n are the charge and concentration for each carrier type. Thus, $\sigma(\omega)$ contains information about the charge carrier dynamics and the temporal behavior of the spreading of electronic states $X^2(t)$.

The Drude-Anderson model assumes a phenomenological expression for the velocity correlation $C(t)$,

$$C(t) \simeq C_C e^{-t/\tau_C} - C_B e^{-t/\tau_B} e^{-t/\tau_\Phi}. \tag{3}$$

The first term corresponds to the standard classical picture of electronic transport, where scattering events lead to a loss of the memory of the initial velocity on a characteristic time τ_C. The second term represents a negative contribution to the velocity correlation function. This corresponds to the backscattering phenomena that is at the heart of the Anderson localization phenomenon. Physically, one must have $\tau_B > \tau_C$ because the backscattering phenomena occurs after several scattering events. The term e^{-t/τ_Φ} describes an exponential damping of the backscattering terms, which is a standard treatment of dephasing processes [36]. In the present case, the dephasing of the backscattering terms is due to the dynamics of the lattice, and τ_Φ is of the order of the period of the LO modes, which are the main source of scattering, i.e., $\tau_\Phi \simeq 1/\omega_E$. In the following, we shall discuss the results by considering mainly the time- and frequency-dependent mobilities defined by

$$\tilde{\mu}(t) = \frac{e}{k_bT}\frac{X^2(t)}{2t}, \qquad \tilde{\mu}(\omega) = \frac{\sigma(\omega)}{ne}, \tag{4}$$

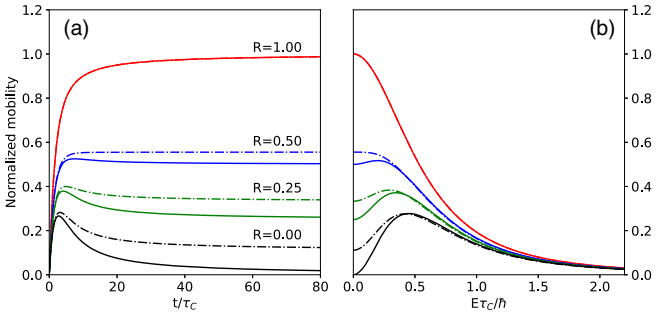

FIG. 2. (a) Normalized time-dependent mobility $\tilde{\mu}(t)/\mu_C$ and (b) normalized frequency-dependent mobility $\tilde{\mu}(\omega)/\mu_C$ for different localization ratio $R = \mu_S/\mu_C$, with (dashed line) or without (full line) dephasing process. Here $\tau_B = 2.5\tau_C$ and $\tau_\phi = 8\tau_B$.

where $e > 0$ is the electron charge and the mobility μ is given by $\mu = \tilde{\mu}(t \to \infty) = \tilde{\mu}(\omega \to 0)$. We define also the static mobility μ_S and the classical mobility μ_C by

$$\mu_S = \frac{e}{k_b T}(C_C\tau_C - C_B\tau_B), \qquad \mu_C = \frac{e}{k_b T}(C_C\tau_C). \quad (5)$$

In the absence of dephasing, i.e., by considering the lattice as static ($\tau_\Phi \to \infty$), one has $\mu = \mu_S$, and the ratio $R = \mu_S/\mu_C$ is an indicator of the importance of localization effects. In Fig. 2 we consider typical regimes of diffusion: one that is classical and presents no localization effect ($R \simeq 1$), one that is strongly localized with ($R \simeq 0$), and two intermediate cases. At short time there is always a ballistic regime during which the charge carrier moves through the material without interacting with disorder, i.e., $\tilde{\mu}(t) \propto t$. The end of this regime marks the elastic diffusion mean free time. It can be followed by a quantum diffusion regime if disorder is strong enough for charge carriers to become localized, inducing a drop in diffusivity and mobility. Finally, at sufficiently large time, the diffusive regime is reached, for which $X^2(t) \propto t$, and the diffusivity and the time-dependent mobility $\tilde{\mu}(t)$ are constant. For a completely localized system, $\tilde{\mu}(t)$ tends exactly to zero at large times. Finally, we emphasize that, when the quantum localization increases, the Drude peak is progressively replaced by a dip in the frequency-dependent conductivity [Fig. 2(b)].

In the presence of dephasing processes, i.e., for a finite τ_Φ, the mobility μ is the sum of the static contribution μ_S and of a contribution due to the lattice dynamics μ_{LD} with

$$\mu = \mu_S + \mu_{\mathrm{LD}}, \qquad \mu_{\mathrm{LD}} = \frac{e}{k_b T}\frac{L^2(\tau_\Phi)}{2\tau_\Phi}. \quad (6)$$

Since lattice dynamics tends to break quantum localization, μ_{LD} is positive with $L^2(\tau_\Phi) = 2C_B\tau_B^2/(1 + \tau_B/\tau_\Phi)$. In the classical limit, there is no backscattering, $C_B = 0$ and $\mu_{\mathrm{LD}} = 0$. In the weak-localization regime, there is some backscattering, and μ_{LD} gives a correction to the static mobility μ_S. In the strongly localized limit $\mu_S \simeq 0$, but transport is still possible thanks to the $\mu_{\mathrm{LD}} > 0$ term. In this regime and in the limit of large τ_Φ, $L(\tau_\Phi)$ is essentially equal to the localization length (see Supplemental Material [26]). The physical picture is that the charge can diffuse up to a maximum extent, which is the localization length. Then diffusion stops and can start again only if a dephasing process breaks the electronic coherence, that is, after a sufficiently large atomic displacement. The physical picture of the dephasing process corresponds to the so-called Thouless regime [37–41] that is expected to occur near a metal-insulator transition. It is also related to the concept of transient localization that has been proposed for crystalline organic semiconductors like rubrene [42–45]. This can also be seen as a process of diffusion that follows nearly adiabatically the evolution of the electrostatic potential. Indeed, in this regime, the typical time needed for localization τ_B is much smaller than the typical time of vibrations τ_Φ and the charge carrier is always close to its state of maximum extension. Therefore, the diffusion is driven by the lattice dynamics, and the diffusion coefficient increases linearly with the vibration frequency $\omega_E \propto 1/\tau_\phi$. Let us emphasize that diffusion results from a dephasing process that differs from the thermally activated hopping regime. We add that in this scenario the mobility decreases when the temperature increases, just as in a bandlike conduction regime. Indeed, increasing temperature, and therefore static disorder, decreases the localization length and $L^2(\tau_\Phi)$ without changing τ_Φ. From Eq. (6) this decreases μ_{LD}. A numerical study of the temperature dependence for MAPI confirms this, as shown below.

We come now to the study of charge carrier mobilities. By applying the real-space Kubo-Greenwood method [16–19], we compute the quantum diffusion $X^2(t)$ and the time-dependent mobility $\tilde{\mu}(t)$ without resorting to perturbative treatment of disorder (see Supplemental Material [26]). As shown previously, holes and electrons have similar mobilities and we present in Fig. 3 values of the time- and frequency-dependent mobilities averaged over electrons and holes states. We emphasize that the optical conductivity, obtained from the frequency-dependent mobility, reflects the dynamics of the charge diffusion and can provide much information [46–48], as shown in Fig. 2.

The model with $\omega_E = 10$ meV is expected to be the closest to perfect bulk MAPI, $\omega_E = 12.5$ meV is a high expectation value, and $\omega_E = 7.5$ meV describes a more imperfect MAPI sample with extrinsic disorder. As shown in Fig. 3, the Drude-Anderson model fits the numerical data of $\tilde{\mu}(t)$ very accurately, which allows us to derive fundamental transport parameters (see Supplemental Material [26]). We find that the LO phonon modes of MAPI limit the mobilities to maximum values of about 200 $\mathrm{cm}^2/(\mathrm{V\,s})$. This result is consistent with recent work [13], which finds strong scattering by LO phonon modes and mobilities of the order of 50–100 $\mathrm{cm}^2/\mathrm{V\,s}$. However, we find that

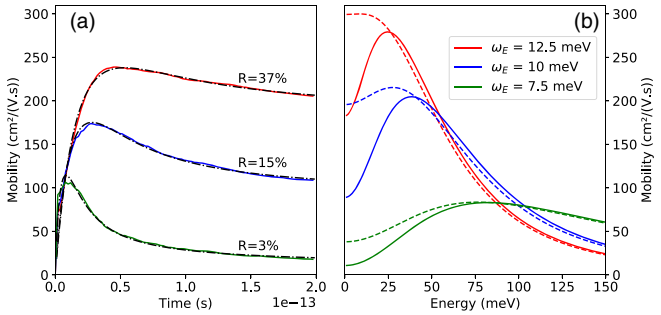

FIG. 3. (a) Mobility $\tilde{\mu}(t)$ as a function of time for different values of ω_E (full line) and the corresponding fits using the Drude-Anderson model (black dashed line). The ratio $R = \mu_S/\mu_C$ is obtained from the fitted parameters. (b) Mobility $\tilde{\mu}(\omega)$ as a function of energy $\hbar\omega$ calculated without dephasing processes (full line) and with a dephasing time $\tau_\phi = 1/\omega_E$ (dotted line). The mobility of the system is $\mu = \tilde{\mu}(t \to \infty) = \tilde{\mu}(\omega \to 0)$. Note that for $\omega_E = 10$ meV μ_S and μ_{LD} contributions to the total mobility μ are nearly equal.

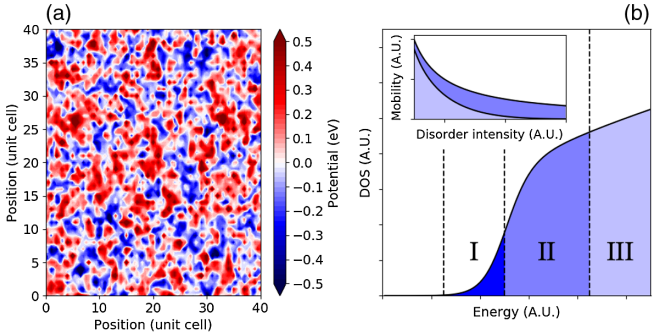

FIG. 4. (a) Variation with position of the electric potential on a planar cut. (b) Energy ranges where different transport mechanisms dominate. I, diffusion dominated by thermally activated hopping. II, diffusion is through the dephasing processes induced by the lattice dynamics. III, bandlike diffusion. (Inset) Schematic representation of the evolution of the mobility $\mu = \mu_S + \mu_{\mathrm{LD}}$ as a function of disorder. Static contribution μ_S (light blue) and lattice driven mobility μ_{LD} (dark blue) are shown.

quantum localization effects are strong, with $R \simeq 0.15$ and comparable contributions of μ_S and μ_{LD}. This differs from [13], which is based on the Boltzmann transport formalism that neglects quantum localization effects. For $\omega_E =$ 10 meV (respectively, $\omega_E = 12.5$ meV), the elastic mean free path $l = \sqrt{\Delta X^2(\tau_C)}$ is about 20 Å (respectively, 30 Å), and the scattering times τ_C are about 8.3 fs (respectively, 10.3 fs). As expected, the backscattering times τ_B are 2–3 times larger than τ_C.

The case $\omega_E = 7.5$ meV is equivalent to an increase of about 30% of the disorder potential with respect to $\omega_E = 10$ meV. The scattering time is $\tau_C \simeq 2.6$ fs, and a large portion of the charge carrier states close to the band edges are strongly localized on a timescale $\tau_B \simeq 8$ fs, which is short compared to the phonon period (of about 400 fs). Figure 3 shows that for this disorder the mobility is around $\mu \simeq 50$ cm^2/V s, with $\mu_S \simeq 10$ and $\mu_{\mathrm{LD}} \simeq 40$ cm^2/V s. The maximum of optical conductivity occurs around 100 meV, which is comparable to results on MAPI films, although it is interpreted by a polaronic state in Ref. [46].

The above results allow us to discuss the formation of large polarons at room temperature. The coupling constant $\alpha \simeq 2$–3 implies the formation of large polarons at low temperatures. The formation energy of the polaron is given by $E_{\mathrm{pol}} \simeq \alpha\hbar\omega_E \simeq 30$ meV [6,7]. Yet, above the Debye temperature (175 K in MAPI [8]), the phonon modes are thermally excited, and this induces a scattering of electrons and a tendency to erase the polaronic state. This is shown, for example, by recent theoretical calculations in the case of CsPbBr3 [49]. This scattering remains delicate to compute with standard polaron theories [50,51]. The scattering by thermal vibrations induces an energy broadening $\Delta E \simeq \hbar/\tau$, where τ is the electron lifetime. In our case, due to the long-range nature of the scattering by longitudinal modes, there is forward scattering, and $\tau \leq \tau_C$. Then, for the systems with highest mobilities $\mu \simeq 200$ cm^2/V s, the energy broadening is $\Delta E \geq \hbar/\tau_C \geq 90$meV. Therefore, even for this less disordered case, the energy broadening due to the scattering by disorder is larger than the polaron formation energy, $\Delta E > E_{\mathrm{pol}}$. Correlatively the estimated polaron radius, of about 40–50 Å, is larger than the elastic mean free path, which is less than 20–30 Å. This indicates that, because of the moderate coupling constant $\alpha \simeq 2$–3, the polaron state is erased by the strong disorder that exists at room temperature. This justifies the starting assumption of the present model that consists to neglect, at sufficiently high temperature, the action of the charge carrier on the lattice and just retain the action of the lattice on the charge carrier.

Finally, we considered the temperature dependence of the mobility in the 300–400 K temperature range. We find that the mobility decreases with increasing temperature (see Supplemental Material [26]), which is in agreement with experimental results. The law $\mu \propto T^{-3/2}$ that is often mentioned in the literature [52] is roughly obeyed. These first results show that the experimental data, which are often considered as an indication of standard bandlike transport, are also consistent with strong quantum localization effects.

Figure 4 summarizes the scenario that is supported by the present Letter. Figure 4(a) shows an instantaneous configuration of the disordered potential, which tends to create localized states. As shown in Fig. 4(b), for an instantaneous potential disorder, extended states, in energy range III, are separated by a mobility edge from localized states, in energy range II and I. For the localized states closest to the mobility edge (region II), the mobility is induced by the dephasing process described in this Letter, with charge carriers following nearly adiabatically the evolution of the electrostatic potential. Farther from the mobility edge (energy range I), one expects that the diffusion will be

dominated by thermally activated hopping, as is usual in disordered systems. The transitions between the different energy regions are expected to be progressive due to the dynamic disorder. We suggest that the small Urbach energy ($E_U \leq 15$ meV) that is measured in MAPbI3 could be related to region I. The inset of Fig. 4(b) shows a qualitative behavior of the mobility μ, and of its static μ_S and dynamic μ_{LD} components, when disorder increases.

To conclude, the present Letter indicates a strong Fröhlich scattering, which induces important quantum localization effects in MAPbI3. The quantum localization that we predict can appear experimentally similar to a large polaronic effect, but is induced by the strong potential disorder. Indeed, we find that the large polaron is not stable at room temperature, because its formation energy is small compared to the energy broadening of disorder. The maximum mobility at room temperature, i.e., without extrinsic disorder, is about 200 $\mathrm{cm}^2/\mathrm{V\,s}$ for both electrons and holes. With additional extrinsic disorder, we find that a large fraction of electrons and holes are localized. Yet these charges can diffuse because they adapt nearly adiabatically to the time evolution of the electrostatic potential. We find that for mobilities below $\mu_c \simeq 50$ $\mathrm{cm}^2/\mathrm{V\,s}$ the electronic diffusion is mainly due to this process. Finally, we believe that the quantum localization demonstrated here could have a profound effect on other properties of MAPI, such as electron-hole recombination, and could also occur in other soft materials, for example, crystalline organic semiconductors [42–45].

We acknowledge fruitful discussions with many colleagues and wish to thank Jacky Even, Claudine Katan, Paulina Plochocka, Julien Delahaye, Dang Le-Si, and Gabriele Davino. We also thank Ghassen Jemai and Kevin-Davis Richler for their help during this study. A. L. is supported by a doctoral grant delivered by the Université Grenoble Alpes.

*antoine.lacroix@neel.cnrs.fr
†guy.trambly@u-cergy.fr
‡pascal.quemerais@neel.cnrs.fr
§jean-pierre.julien@neel.cnrs.fr
‖didier.mayou@neel.cnrs.fr

[1] M. A. Green, A. Ho-Baillie, and H. J. Snaith, The emergence of perovskite solar cells, Nat. Photonics **8**, 506 (2014), review article.
[2] J. S. Manser, J. A. Christians, and P. V. Kamat, Intriguing optoelectronic properties of metal halide perovskites, Chem. Rev. **116**, 12956 (2016).
[3] L. D. Whalley, J. M. Frost, Y.-K. Jung, and A. Walsh, Perspective: Theory and simulation of hybrid halide perovskites, J. Chem. Phys. **146**, 220901 (2017).
[4] C.-J. Yu, Advances in modelling and simulation of halide perovskites for solar cell applications, J. Phys. Energy **1**, 022001 (2019).
[5] A. J. Neukirch, W. Nie, J.-C. Blancon, K. Appavoo, H. Tsai, M. Y. Sfeir, C. Katan, L. Pedesseau, J. Even, J. J. Crochet, G. Gupta, A. D. Mohite, and S. Tretiak, Polaron stabilization by cooperative lattice distortion and cation rotations in hybrid perovskite materials, Nano Lett. **16**, 3809 (2016).
[6] J. M. Frost, L. D. Whalley, and A. Walsh, Slow cooling of hot polarons in halide perovskite solar cells, ACS Energy Lett. **2**, 2647 (2017).
[7] C. Wolf, H. Cho, Y.-H. Kim, and T.-W. Lee, Polaronic charge carrier-lattice interactions in lead halide perovskites, ChemSusChem **10**, 3705 (2017).
[8] J. Feng, Mechanical properties of hybrid organic-inorganic $ch_3nh_3pbi_3$ ($b = sn, pb; x = br, i$) perovskites for solar cell absorbers, APL Mater. **2**, 081801 (2014).
[9] L. D. Whalley, J. M. Skelton, J. M. Frost, and A. Walsh, Phonon anharmonicity, lifetimes, and thermal transport in $ch_3nh_3pbi_3$ from many-body perturbation theory, Phys. Rev. B **94**, 220301(R) (2016).
[10] M. A. Pérez-Osorio, R. L. Milot, M. R. Filip, J. B. Patel, L. M. Herz, M. B. Johnston, and F. Giustino, Vibrational properties of the organic-inorganic halide perovskite $ch_3nh_3pbi_3$ from theory and experiment: Factor group analysis, first-principles calculations, and low-temperature infrared spectra, J. Phys. Chem. C **119**, 25703 (2015).
[11] M. Baranowski, J. M. Urban, N. Zhang, A. Surrente, D. K. Maude, Z. Andaji-Garmaroudi, S. D. Stranks, and P. Plochocka, Static and dynamic disorder in triple-cation hybrid perovskites, J. Phys. Chem. C **122**, 17473 (2018).
[12] A. D. Wright, C. Verdi, R. L. Milot, G. E. Eperon, M. A. Pérez-Osorio, H. J. Snaith, F. Giustino, M. B. Johnston, and L. M. Herz, Electron-phonon coupling in hybrid lead halide perovskites, Nat. Commun. **7**, 11755 (2016), article.
[13] S. Poncé, M. Schlipf, and F. Giustino, Origin of low carrier mobilities in halide perovskites, ACS Energy Lett. **4**, 456 (2019).
[14] L. Martiradonna, Riddles in perovskite research, Nat. Mater. **17**, 377 (2018).
[15] W. Li, A. S. Vasenko, J. Tang, and O. V. Prezhdo, Anharmonicity extends carrier lifetimes in lead halide perovskites at elevated temperatures, J. Phys. Chem. Lett. **10**, 6219 (2019).
[16] D. Mayou, Calculation of the conductivity in the short-mean-free-path regime, Europhys. Lett. **6**, 549 (1988).
[17] D. Mayou and S. Khanna, A real-space approach to electronic transport, J. Phys. I **5**, 1199 (1995).
[18] S. Roche and D. Mayou, Conductivity of Quasiperiodic Systems: A Numerical Study, Phys. Rev. Lett. **79**, 2518 (1997).
[19] F. Triozon, J. Vidal, R. Mosseri, and D. Mayou, Quantum dynamics in two- and three-dimensional quasiperiodic tilings, Phys. Rev. B **65**, 220202(R) (2002).
[20] S. Fratini, S. Ciuchi, and Didier Mayou, Phenomenological model for charge dynamics and optical response of disordered systems: Application to organic semiconductors, Phys. Rev. B **89**, 235201 (2014).
[21] S. Boyer-Richard, C. Katan, B. Traoré, R. Scholz, J.-M. Jancu, and J. Even, Symmetry-based tight binding modeling of halide perovskite semiconductors, J. Phys. Chem. Lett. **7**, 3833 (2016).
[22] F. Brivio, K. T. Butler, A. Walsh, and M. van Schilfgaarde, Relativistic quasiparticle self-consistent electronic structure

of hybrid halide perovskite photovoltaic absorbers, Phys. Rev. B **89**, 155204 (2014).
[23] T. Ahmed, C. La o vorakiat, T. Salim, Y. M. Lam, E. E. M. Chia, and J.-X. Zhu, Optical properties of organometallic perovskite: An ab initio study using relativistic GW correction and Bethe-Salpeter equation, Europhys. Lett. **108**, 67015 (2014).
[24] T. A. Tyson, W. Gao, Y.-S. Chen, S. Ghose, and Y. Yan, Large thermal motion in halide perovskites, Sci. Rep. **7**, 9401 (2017).
[25] J. C. Slater and G. F. Koster, Simplified lcao method for the periodic potential problem, Phys. Rev. **94**, 1498 (1954).
[26] See Supplemental Material at http://link.aps.org/supplemental/10.1103/PhysRevLett.124.196601 for a more detailed description of the model, as well as a discussion of the effect of MA cations, phonon modes, and temperature, which includes Refs. [27–31].
[27] F. Brivio, J. M. Frost, J. M. Skelton, A. J. Jackson, O. J. Weber, M. T. Weller, A. R. Goñi, A. M. A. Leguy, P. R. F. Barnes, and A. Walsh, Lattice dynamics and vibrational spectra of the orthorhombic, tetragonal, and cubic phases of methylammonium lead iodide, Phys. Rev. B **92**, 144308 (2015).
[28] C. Grote and R. F. Berger, Strain tuning of tin-halide and lead-halide perovskites: A first-principles atomic and electronic structure study, J. Phys. Chem. C **119**, 22832 (2015).
[29] R. Prasanna, A. Gold-Parker, T. Leijtens, B. Conings, A. Babayigit, H.-G. Boyen, M. F. Toney, and M. D. McGehee, Band gap tuning via lattice contraction and octahedral tilting in perovskite materials for photovoltaics, J. Am. Chem. Soc. **139**, 11117 (2017).
[30] S. Govinda, B. P. Kore, M. Bokdam, P. Mahale, A. Kumar, S. Pal, B. Bhattacharyya, J. Lahnsteiner, G. Kresse, C. Franchini, A. Pandey, and D. D. Sarma, Behavior of methylammonium dipoles in mapbx3 ($x = br$ and i), J. Phys. Chem. Lett. **8**, 4113 (2017).
[31] N. P. Gallop, O. Selig, G. Giubertoni, H. J. Bakker, Y. L. A. Rezus, J. M. Frost, T. L. C. Jansen, R. Lovrincic, and A. A. Bakulin, Rotational cation dynamics in metal halide perovskites: Effect on phonons and material properties, J. Phys. Chem. Lett. **9**, 5987 (2018).
[32] F. Brivio, K. T. Butler, A. Walsh, and M. van Schilfgaarde, Relativistic quasiparticle self-consistent electronic structure of hybrid halide perovskite photovoltaic absorbers, Phys. Rev. B **89**, 155204 (2014).
[33] S. E. Skipetrov and I. M. Sokolov, Ioffe-Regel criterion for anderson localization in the model of resonant point scatterers, Phys. Rev. B **98**, 064207 (2018).
[34] S. Fratini, S. Ciuchi, D. Mayou, G. Trambly de Laissardière, and A. Troisi, A map of high-mobility molecular semiconductors, Nat. Mater. **16**, 998 (2017).
[35] T. Nematiaram, S. Ciuchi, X. Xie, S. Fratini, and A. Troisi, Practical computation of the charge mobility in molecular semiconductors using transient localization theory, J. Phys. Chem. C **123**, 6989 (2019).
[36] P. A. Lee and T. V. Ramakrishnan, Disordered electronic systems, Rev. Mod. Phys. **57**, 287 (1985).
[37] Y. Imry, Possible Role of Incipient Anderson Localization in the Resistivities of Highly Disordered Metals, Phys. Rev. Lett. **44**, 469 (1980).
[38] J. Delahaye, C. Berger, and G. Fourcaudot, Thouless and critical regimes in insulating icosahedral AlPdRe ribbons, J. Phys. Condens. Matter **15**, 8753 (2003).
[39] Z. Ovadyahu, Some finite temperature aspects of the anderson transition, J. Phys. C **19**, 5187 (1986).
[40] J. Delahaye and C. Berger, The question of intrinsic origin of the metal-insulator transition in i-alpdre quasicrystal, Eur. Phys. J. B **88**, 102 (2015).
[41] G. Trambly de Laissardière, J.-P. Julien, and D. Mayou, Quantum Transport of Slow Charge Carriers in Quasicrystals and Correlated Systems, Phys. Rev. Lett. **97**, 026601 (2006).
[42] A. Troisi, Charge transport in high mobility molecular semiconductors: Classical models and new theories, Chem. Soc. Rev. **40**, 2347 (2011).
[43] S. Ciuchi, S. Fratini, and D. Mayou, Transient localization in crystalline organic semiconductors, Phys. Rev. B **83**, 081202(R) (2011).
[44] S. Fratini, D. Mayou, and S. Ciuchi, The transient localization scenario for charge transport in crystalline organic materials, Adv. Funct. Mater. **26**, 2292 (2016).
[45] A. Missaoui, J. Khabthani, G. Trambly de Laissardière, and D. Mayou, Two-dimensional electronic transport in rubrene: The impact of inter-chain coupling, Entropy **21**, 233 (2019).
[46] K. T. Munson, E. R. Kennehan, G. S. Doucette, and J. B. Asbury, Dynamic disorder dominates delocalization, transport, and recombination in halide perovskites, Chem **4**, 2826 (2018).
[47] L. Luo, L. Men, Z. Liu, Y. Mudryk, X. Zhao, Y. Yao, J. M. Park, R. Shinar, J. Shinar, K.-M. Ho, I. E. Perakis, J. Vela, and J. Wang, Ultrafast terahertz snapshots of excitonic Rydberg states and electronic coherence in an organometal halide perovskite, Nat. Commun. **8**, 15565 (2017).
[48] D. A. Valverde-Chávez, C. S. Ponseca, C. C. Stoumpos, A. Yartsev, M. G. Kanatzidis, V. Sundström, and D. G. Cooke, Intrinsic femtosecond charge generation dynamics in single crystal $ch_3nh_3pbi_3$, Energy Environ. Sci. **8**, 3700 (2015).
[49] M. Bernardi (private communication).
[50] F. M. Peeters and J. T. Devreese, *Theory of Polaron Mobility* (Academic Press, New York, 1984) pp. 81–133.
[51] J. Moore Frost, Calculating polaron mobility in halide perovskites, Phys. Rev. B **96**, 195202 (2017).
[52] R. L. Milot, G. E. Eperon, H. J. Snaith, M. B. Johnston, and L. M. Herz, Temperature-dependent charge-carrier dynamics in $ch_3nh_3pbi_3$ perovskite thin films, Adv. Funct. Mater. **25**, 6218 (2015).